Baroclinic Flow over a Mountain Ridge

PETER R. BANNON

Department of Meteorology, The Pennsylvania State University, University Park, Pennsylvania

JOSEPH A. ZEHNDER

Institute of Atmospheric Physics, University of Arizona, Tucson, Arizona

(Manuscript received 28 April 1988, in final form 30 September 1988)

ABSTRACT

Flow incident on a mountain ridge with a linear vertical windshear is studied for a Boussinesq, adiabatic, inviscid fluid on the *f*-plane. A scale analysis indicates that the semigeostrophic approximation of a geostrophic mountain-parallel wind holds for sufficiently shallow mountain slopes if the Rossby number squared is small. In such a limit, the equation for the vertical displacement of a fluid parcel is elliptic if there is forward shear (wind increasing with height) or weak backward shear (wind decreasing with height) but hyperbolic if there is strong backward shear such that the incident wind vanishes at some level in the flow.

Steady-state results indicate that forward shear weakens the cold-core geostrophic mountain anticyclone predicted by barotropic theory while weak backshear strengthens it. This behavior arises from the warm- (cold-) air advection in the forward (backward) shear case. While the total ageostrophic flux of mass across the mountain peak is greater for the forward shear case, the maximum ageostrophic cross-mountain wind is less.

Results for the semigeostrophic initial-value problem with a critical level depict the development of a stronger and narrower baroclinic lee trough than for quasi-geostrophic theory.

1. Introduction

Theoretical studies of lee cyclogenesis have led to a variety of explanations of the phenomenon. Mattocks and Bleck (1986) provide a recent survey of the literature. While some theories focus on the interaction of a growing baroclinic wave *disturbance* with the topography (e.g., Pierrehumbert 1985), others emphasize that lee cyclogenesis is primarily associated with the interaction of the large-scale baroclinic *flow* with the mountain range. For example, Merkine (1975) found that the shear of a baroclinic flow is increased downstream of a mountain ridge, and suggested that cyclogenesis would be preferred in the lee. Smith (1984) noted that shear flow over a mountain with a critical level would produce a nonsingular resonance of an Eady edge wave. Recently Hayes et al. (1987) advanced a superposition theory in which the mountain anticyclone of the steady state solution masks the presence of a growing baroclinic disturbance which appears to intensify in the lee of the mountain.

It is clear that a thorough analysis of synoptic- and mesoscale orographic flows in a baroclinic environment is required to improve our understanding of lee cyclogenesis and related problems (e.g., frontal propagation over mountains). Toward such an understanding, the present study describes both geostrophic and ageostrophic fields for a rotating, uniformly sheared flow incident on a mountain ridge. The model utilizes the approach of Robinson (1960) to extend quasi-geostrophic theory to include finite amplitude topography.

Merkine (1975) first examined the shear flow problem and derived the far-field behavior. Solutions near the mountain were only obtained for the case of uniform flow. Blumen and Gross (1986) presented complete solutions subject to the unrealistic constraint of an isentropic lower boundary. As is demonstrated below, however, this simplification fails to capture the essence of the baroclinic flow problem. Hayes et al. (1987) solved the problem with a linearized lower boundary condition and periodicity in the west–east direction. We note that the assumption of zonal periodicity is inconsistent with the presence of a permanent turning of the flow. The present study eliminates these shortcomings, but, like the other analyses, is restricted to a rectilinear shear with no backing or veering of the wind with height.

The next section describes the model physics and its mathematical representation. A scale analysis of the basic equations determines the nondimensional parameters of the flow and provides justification for the semigeostrophic assumption that the mountain-parallel flow is in geostrophic balance. Section 3 derives the governing equation of the flow following the approach

Corresponding author address: Dr. Peter R. Bannon, Dept. of Meteorology, Pennsylvania State University, 503 Walker Building, University Park, PA 16802.

of Bannon and Chu (1988, henceforth denoted as BC). It is shown that this equation is elliptic if the incident wind does not reverse direction with height. Sections 4 and 5 discuss the consequences of the drag and lift forces on the flow. Section 6 describes the flow solution to the elliptic problem when there is no reversal in the incident wind direction. Section 7 presents results to the initial value problem when there is a wind reversal. Some conclusions and their implications are discussed in section 8.

2. The model

The basic-state model atmosphere consists of an inviscid, Boussinesq fluid with uniform buoyancy frequency N. A mountain ridge of width a and height h_0 lies at the origin of a rotating Cartesian coordinate system with constant Coriolis parameter f. A flow with uniform windshear is incident on the mountain with surface components U_0 normal and V_0 parallel to the ridge. A rigid lid at a height D models the tropopause. Figure 1 summarizes the model physics and geometry.

a. Basic equations

The equations describing the adiabatic hydrostatic flow are

$$\frac{Du}{Dt} - fv = -\frac{\partial \phi}{\partial x}, \tag{2.1a}$$

$$\frac{Dv}{Dt} + fu = -\frac{\partial \phi}{\partial y}, \tag{2.1b}$$

$$\frac{\partial \phi}{\partial z} = g\frac{\delta\theta}{\theta_0}, \tag{2.1c}$$

$$\frac{\partial u}{\partial x} + \frac{\partial v}{\partial y} + \frac{\partial w}{\partial z} = 0, \tag{2.1d}$$

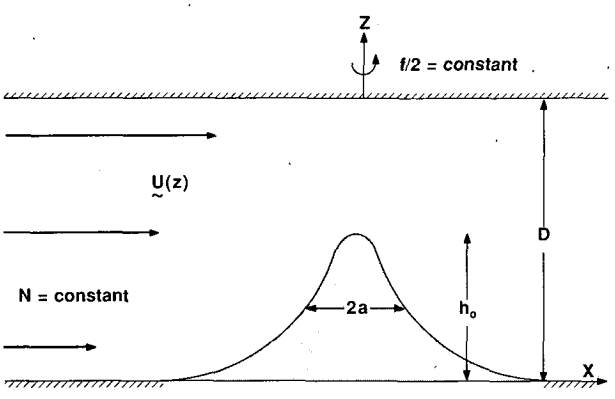

FIG. 1. Schematic illustration of the model. An infinitely long mountain ridge of height h_0 and characteristic width a lies at the center of a Cartesian coordinate system. The basic state atmosphere has constant buoyancy frequency N and constant Coriolis parameter f. A rigid-lid tropopause lies at a height D. Far upstream a flow with linear windshear $\mathbf{U}(z) = U_0(1 + \alpha z)$ is incident on the mountain.

$$\frac{D}{Dt}\left(N^2 z + g\frac{\delta\theta}{\theta_0}\right) = 0, \tag{2.1e}$$

where

$$\frac{D}{Dt} = \frac{\partial}{\partial t} + u\frac{\partial}{\partial x} + v\frac{\partial}{\partial y} + w\frac{\partial}{\partial z}. \tag{2.2}$$

Here $\delta\theta$ is the dynamic contribution to the potential temperature, θ_0 is a reference temperature, (u, v, w) is the velocity vector and the geopotential ϕ is related to the pressure p and density ρ by $\phi = p/\rho$. The vertical boundary conditions on the flow are

$$w = \frac{Dh}{Dt} \quad \text{at} \quad z = h(x), \tag{2.3a}$$

$$w = 0 \quad \text{at} \quad z = D, \tag{2.3b}$$

where h is the mountain profile. The latter condition reflects the assumption of a rigid lid aloft.

We write the steady solution as the sum of the incident flow and that induced by the mountain:

$$u = (U_0 + \alpha z) + u_a'(x, z), \tag{2.4a}$$

$$v = \tau(U_0 + \alpha z) + v'(x, z), \tag{2.4b}$$

$$w = w'(x, z), \tag{2.4c}$$

$$\phi = f(U_0 + \alpha z)(\tau x - y) + \phi'(x, z), \tag{2.4d}$$

$$g\frac{\delta\theta}{\theta_0} = f\alpha(\tau x - y) + g\frac{\delta\theta'}{\theta_0}(x, z). \tag{2.4e}$$

The primed fields denote the mountain induced disturbance and, since $h = h(x)$, are independent of y. The subscript a denotes an ageostrophic wind component. The geostrophic incident flow has constant linear shear α with angle of attack $\tan^{-1}(\tau = V_0/U_0)$.

b. Scale analysis

Following BC, we choose the mountain width, a, as the characteristic length scale and the associated deformation depth $H_R = fa/N$ as the characteristic vertical scale. Based on the lower boundary condition and the a priori assumption that the mountain parallel flow will be in thermal wind balance, we introduce the following scaling:

$$x = ax'', \quad z = H_R z'', \quad h = h_0 h''(x), \tag{2.5a}$$

$$u = U_0(\hat{u} + \mu u_a''), \quad D = H_R z_T'', \tag{2.5b}$$

$$v = \tau U_0 \hat{u} + N h_0 v'', \quad \phi' = N f a h_0 \phi'', \tag{2.5c}$$

$$w' = U_0\frac{f}{N}\mu w'', \quad g\frac{\delta\theta'}{\theta_0} = N^2 h_0 \theta'', \tag{2.5d}$$

where the double primed quantities are nondimensional and the scaled incident zonal wind is

$$\hat{u} = 1 + \gamma z''. \tag{2.6}$$

Here $\gamma = \alpha H_R/U_0$ is the nondimensionalized shear such that a value of unity indicates a doubling of the incident wind from its surface value in one deformation depth. The parameter $\mu = h_0/H_R$ is a nondimensional measure of the strength of the topography and of the ageostrophic motion it induces.

Substituting (2.4)–(2.6) into (2.1) and (2.3) yields, upon dropping the double primes,

$$-v = -\frac{\partial \phi}{\partial x}, \tag{2.7a}$$

$$\frac{dv}{dt} + \gamma \epsilon w + u_a = 0, \tag{2.7b}$$

$$\frac{\partial \phi}{\partial z} = \theta, \tag{2.7c}$$

$$\frac{\partial u}{\partial x} + \mu \frac{\partial w}{\partial z} = 0, \tag{2.7d}$$

$$\frac{d}{dt}(z + \mu\theta) + \gamma\mu(\epsilon u_a - v) = 0, \tag{2.7e}$$

where

$$\frac{d}{dt} = (\hat{u} + \mu u_a)\frac{\partial}{\partial x} + \mu w \frac{\partial}{\partial z}, \tag{2.7f}$$

and

$$w = \begin{cases} \dfrac{dh}{dt} & \text{at} \quad z = \mu h \qquad (2.8a) \\ 0 & \text{at} \quad z = z_T. \qquad (2.8b) \end{cases}$$

Table 1 defines the five nondimensional parameters describing the flow.

c. *Validity of the semigeostrophic approximation*

In writing the zonal momentum equation, (2.7a), we have made the semigeostrophic approximation that the mountain-parallel wind is in geostrophic balance. The terms neglected in (2.7a) represent the advection of zonal momentum:

$$\mathrm{Ro}^2\left(\frac{du_a}{dt} + \gamma w\right). \tag{2.9}$$

This approximation is valid provided the square of the Rossby number Ro of the flow is small and that the shear and topography are not large:

$$\mathrm{Ro}^2 \ll 1,$$

$$O(\gamma, \mu) \lesssim 1. \tag{2.10}$$

Numerical solutions presented in sections 6 and 7 suggest that (2.10) can overestimate the range of validity of the semigeostrophic approximation, particularly in the case of back shear, $\gamma < 0$. Inspection of (2.7) and (2.8) indicates that the semigeostrophic problem depends on μ, z_T, γ and ϵ but is not a function of the incident normal windspeed U_0. It is straightforward (e.g., Bannon and Chu 1988) to show that this set reduces to the quasi-geostrophic problem in the limit as μ and ϵ tend to zero.

TABLE 1. Nondimensional flow parameters.

$\mu = h_0/H_R = Nh_0/fa$
$\gamma = \alpha H_R/U_0$
$\mathrm{Ro} = U_0/fa$
$\epsilon = \tau\,\mathrm{Ro} = V_0/fa$
$z_T = D/H_R$

3. Governing equation and method of solution

a. *Equation for vertical streamline displacement*

The techniques developed in BC are applied to the present baroclinic problem to derive a second-order partial differential equation for the vertical displacement of the streamlines. Derivation of the governing equation follows section 3a of BC closely with $\hat{\rho} = 1$ and $\hat{u} = 1 + \gamma z$, and the reader is referred to that study for the details of the analysis. A streamfunction, ψ,

$$u = \frac{\partial \psi}{\partial z}, \quad \mu w = -\frac{\partial \psi}{\partial x}, \tag{3.1}$$

satisfies mass continuity and enables a convective derivative to be represented by, for example,

$$v = \frac{d\eta}{dt} = J(\psi, \eta), \tag{3.2}$$

where $J(\psi, \eta) = \hat{y}\cdot(\nabla\psi \times \nabla\eta)$ is the Jacobian and $\eta(x, z)$ is the meridional displacement of a fluid parcel.

Conservation of potential temperature may be expressed as

$$(1 - \gamma^2\epsilon^2)z + \mu\theta - \gamma\mu(\eta + \epsilon v) = (1 - \gamma^2\epsilon^2)z_\infty(\psi), \tag{3.3}$$

using (2.7b), (2.7e), (3.2) and the definition

$$\mu w = J(\psi, z). \tag{3.4}$$

The function

$$z_\infty(\psi) = [-1 + \sqrt{1 + 2\gamma\psi}]/\gamma, \tag{3.5}$$

is the height of a streamline far upstream of the mountains where $\psi = z + \gamma z^2/2$. The thermal wind relation may be written as

$$\frac{\partial v}{\partial z} = \frac{1}{\mu}\frac{\partial \Theta}{\partial x}, \tag{3.6}$$

where

$$\Theta = (1 - \gamma^2\epsilon^2)z_\infty(\psi) + \gamma\mu(\eta + \epsilon v), \tag{3.7a}$$

or

$$\Theta = (1 - \gamma^2\epsilon^2)z + \mu\theta. \tag{3.7b}$$

Introduction of a streamfunction coordinate system (χ, ψ) where

$$\chi = x, \quad \psi = \psi(x, z), \tag{3.8}$$

makes the streamfunction height $z = z(\chi, \psi)$ the new dependent variable. Following BC, an equation for z is found to be

$$\frac{\partial}{\partial\chi}\left(\frac{\partial\Theta}{\partial\psi}\frac{\partial z}{\partial\chi}\right) - \frac{\partial}{\partial\chi}\left[\left(\frac{\partial\Theta}{\partial\chi} + \gamma\epsilon\right)\frac{\partial z}{\partial\psi}\right] + \frac{\partial}{\partial\psi}\left(\hat{u}\frac{\partial z}{\partial\psi}\right) = 0, \tag{3.9}$$

with the boundary conditions

$$z = \mu h \quad \text{at} \quad \psi = 0, \tag{3.10a}$$

$$z = z_T \quad \text{at} \quad \psi = z_T + \gamma z_T^2/2. \tag{3.10b}$$

Equation (3.9) is the governing equation for the vertical displacement z of a fluid parcel in (χ, ψ) space for baroclinic flow. The barotropic version of (3.9) has been solved by Robinson (1960), Jacobs (1964), Merkine (1975) and Pierrehumbert (1985). Equation (3.9) is elliptic provided

$$\frac{\hat{u}(\partial\Theta/\partial\psi)}{(\partial\Theta/\partial\chi + \gamma\epsilon)^2} > \frac{1}{4}, \tag{3.11}$$

indicating that the effective Richardson number of the flow in (χ, ψ) space be greater than ¼. For stably stratified flow, $\partial\Theta/\partial\psi > 0$, condition (3.11) is violated if $\hat{u} = 0$. This result is the semigeostrophic extension of the quasi-geostrophic case (Smith 1984).

b. *Solution for the elliptic problem*

In the case of forward shear or weak backward shear such that no critical level exists in the flow, (3.9) is elliptic and we adopt the method of BC to obtain a solution. Modifications include a rigid-lid upper boundary condition and a vertical transformation of the form

$$\hat{\psi} = \exp(-\psi/2),$$

which provides a typical vertical grid space of $0.02D$ for 51 grid points. Further details of the iterative method for solving the elliptic equation appear in BC.

c. *Solution for the hyperbolic problem*

In the case of strong backward shear, the incident wind vanishes, (3.9) is hyperbolic and the approach of the preceding section is no longer applicable. Here we treat the problem as an initial value one and obtain solutions using a modified version of the geostrophic momentum model of Zehnder and Bannon (1988, hereafter referred to as ZB).

The model of ZB is based on the advection of potential vorticity in the interior, of potential temperature on the vertical boundaries, and of absolute momentum on the lateral boundaries. The geostrophic flow fields are then diagnosed from the potential vorticity using the principle of invertibility, while the ageostrophic fields are obtained from an elliptic transverse circulation equation. Rather than making the geostrophic coordinate transformation, the equations are solved in physical space using terrain following coordinates.

The numerical domain and techniques used here are identical to that in ZB. The code was modified in a straightforward manner to incorporate a mean wind with shear while the deformation and frontal fields used in ZB were deleted.

4. Permanent turning and the lift force

Jacobs (1964) first noted that a uniform flow of finite depth suffers a permanent meridional deflection to the right (looking downstream) as it crosses the mountain ridge. Merkine (1975) included the effect of shear on the amplitude of this turning. Here we present an alternative derivation which provides additional insight into the turning and which extends the discussion of BC that relates the turning to the lift force acting on the mountain.

The nondimensional net change in the mountain-induced meridional velocity, $\Delta\hat{v}$, is

$$\Delta\hat{v}(z) = v(x = +\infty, z) - v(x = -\infty, z), \tag{4.1}$$

where by definition v vanishes far upstream. Recall that the *total* meridional wind far upstream is $\tau\hat{u}$ and does *not* vanish. Our definition (4.1) for the change in the meridional wind is unaltered if this zonally uniform component is included. We first note that the downstream flow is equivalent-barotropic and that the turning $\Delta\hat{v}$ is proportional to the incident wind field. Far downstream where the ageostrophic motions are assumed to vanish, the heat equation (2.7e) reduces to

$$\hat{u}\frac{\partial\theta}{\partial x} = \gamma v, \tag{4.2}$$

since, by definition, $\hat{u}(z)$ is unchanged downstream. Using the thermal wind relation,

$$\frac{\partial v}{\partial z} = \frac{\partial\theta}{\partial x},$$

in (4.2) we obtain

$$v(x = +\infty, z) = \hat{A}\hat{u}, \tag{4.3}$$

where $\hat{A}$ is a constant. This result can be shown to hold for arbitrary $\hat{u}(z)$. Thus the turning increases linearly with height at a rate given by the incident windshear.

To obtain an expression for $\Delta\hat{v}$, we rewrite the meridional momentum equation (2.7b) using (3.4) in streamfunction coordinates as

$$u\frac{\partial}{\partial \chi}(v + \epsilon\gamma\mu z) = -u_a. \tag{4.4}$$

Introducing an ageostrophic streamfunction, Φ, defined by

$$u_a = \frac{\partial \Phi}{\partial z}, \quad w = -\frac{\partial \Phi}{\partial x}, \tag{4.5}$$

(4.4) becomes

$$\frac{\partial}{\partial \chi}(v + \epsilon\gamma\mu z) = -\left(\frac{\partial \Phi}{\partial z}\right)\Big/\left(\frac{\partial \psi}{\partial z}\right) = -\frac{\partial \Phi}{\partial \psi}, \tag{4.6}$$

and upon integration along a streamline we find

$$\Delta\hat{v} = -\int_{-\infty}^{+\infty} \frac{\partial \Phi}{\partial \psi}\, d\chi, \tag{4.7}$$

since the net change in the vertical displacement of a fluid parcel, Δz, vanishes. This expression indicates that the permanent turning is directly proportional to the ageostrophic flow which accomplishes the turning but inversely proportional to the strength of the lateral flow. Substituting (4.3) into (4.7) and integrating over ψ from the surface, $\psi = 0$, to the top, $\psi = \psi_T = z_T + \gamma z_T^2/2$, yields

$$\hat{A}\int_0^{\psi_T} \hat{u}\, d\psi = \int_{-\infty}^{+\infty} \Phi(\chi, 0)\, d\chi, \tag{4.8}$$

where the order of integration on the right-hand side has been interchanged and $\Phi(\chi, \psi_T) = 0$.

A convenient expression for Φ may be derived as follows. Since $u = \hat{u} + \mu u_a$,

$$\frac{\partial \psi}{\partial z} = (1 + \gamma z) + \mu\frac{\partial \Phi}{\partial z},$$

which implies

$$\Phi = [\psi - (z + \gamma z^2/2)]/\mu,$$

where an arbitrary function of x vanishes in order to be consistent with the upper boundary condition. Noting that $\psi = z_\infty + \gamma z_\infty^2/2$ and letting $z = z + \delta$ where δ is the vertical displacement of a streamline from its position far upstream, we obtain

$$\Phi = -\left[\delta(1 + \gamma z_\infty) + \frac{\gamma\delta^2}{2}\right]\Big/\mu. \tag{4.9}$$

Our expression for $\hat{A}$ then becomes

$$\hat{A} = -\frac{\int_{-\infty}^{+\infty} [h + \gamma\mu h^2/2]\, d\chi}{\int_0^{z_T} \hat{u}^2\, dz}, \tag{4.10}$$

since $\delta(\chi, 0) = \mu h(\chi)$ and $\hat{u} = \partial\psi/\partial z$ at $z = \infty$. This result is consistent with that of Merkine (1975) and represents a finite-amplitude, baroclinic extension of the linear barotropic result of Smith (1979).

In order to interpret (4.10) we note that following BC the dimensional lift force per unit ridge length acting on the mountain is

$$\mathrm{LL} = \int_M \rho f U(z)\, dx dz, \tag{4.11}$$

where the integration is over the cross sectional area of the mountain. The nondimensional lift $\widehat{\mathrm{LL}} = \mathrm{LL}/\rho f U_0 a H_R$ is

$$\widehat{\mathrm{LL}} = \mu\int_{-\infty}^{+\infty} (h + \gamma\mu h^2/2)\, dx. \tag{4.12}$$

Thus, dimensionally, the permanent turning is given by

$$\Delta V = -AU(z), \tag{4.13}$$

where

$$A = +\mathrm{LL}/TMF \tag{4.14}$$

is the ratio of the lift force to the total momentum flux, TMF,

$$TMF = \int_0^{z_T} \rho U^2(z)\, dz. \tag{4.15}$$

We note that the derivation of (4.13) has assumed that the ageostrophic motions vanish far downstream. While this assumption is appropriate for the elliptic case, it is not necessarily valid for the hyperbolic one where a standing lee wave can exist. However, the analysis in the Appendix for the quasi-geostrophic problem indicates that the downstream v field will be composed of both a net mean deflection consistent with (4.13) and sinusoidal components of vanishing mean.

Figure 2 shows the variation of the permanent turning with the mountain height for a Gaussian profile. The dimensional turning is scaled by fa so that

$$\Delta V/fa = \mu\hat{A}\hat{u}. \tag{4.16}$$

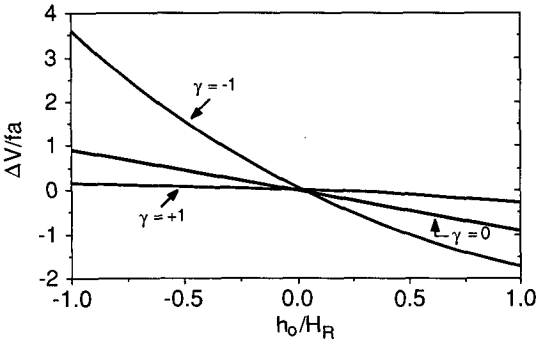

FIG. 2. The permanent turning ΔV (in units of fa) at the surface as a function of the mountain height h_0 scaled by the deformation depth, $H_R = fa/N$, for various values of the nondimensional shear $\gamma = \alpha H_R/U_0$, with $z_T = 2$. The turning increases linearly with height at a rate given by the incident windshear.

Looking downstream a fluid parcel is deflected to the right as it crosses the mountain by the Coriolis force associated with the ageostrophic zonal wind. This deflection is larger for backward shear ($\gamma < 0$) because the reduction in the ageostrophic flow [i.e., the numerator of (4.10)] is overcompensated by the reduction in the incident momentum flux [i.e., the denominator of (4.10)]. In contrast a valley ($\mu < 0$) produces a deflection to the left ($\Delta V > 0$). The amplitude of the turning is decreased (increased) compared to the mountain case when the shear is forward (backward). This difference arises from the quadratic term in μ of the numerator. In all cases we note that the turning tends to zero as the rigid upper lid is moved to infinity, $z_T \to \infty$.

5. Angle of attack and mountain drag

The preceding analysis of the permanent turning emphasized the net change in the meridional velocity. This net deflection of the flow is independent of the angle of attack, measured here by $\tau = V_0/U_0$. Since the meridional flow is assumed to be in geostrophic balance, the dimensional drag per unit ridge length is, using (2.4b),

$$\mathrm{DL} = -\int_M \rho f V(z)\,dx dz - \int_M \rho f v'(x, z)\,dx dz. \quad (5.1)$$

Because of the permanent turning of the flow, v' is generally negative in the vicinity of the mountain, and the second integral in (5.1) makes a positive contribution to the drag. If the flow is steady, no drag is possible for the invicid flow lacking wave motions (Bannon 1985). In such a case $V(z)$ must be chosen so that DL = 0. This is accomplished for $V(z) = +AU(z)/2$ (i.e., $\tau = +A/2$). Such a choice is consistent with the discussion of Smith (1979) who argued and Blumen (1988) who demonstrated that an infinite ridge alters the angle of attack for steady flow. Thus, $V(z)$ in this model reflects that upstream influence of the mountain ridge. The choice $\tau = +A/2$ produces a symmetric v-field and no drag. We note that mathematical solutions for different angles of attack (i.e., $\tau \neq +A/2$) possess a nonzero drag and physically correspond to unsteady solutions with a shed vortex which propagates downstream. Locally over the mountain, however, the flow would be time independent.

6. Solutions for forward and weak backward shear

When the incident wind increases with height or decreases sufficiently slowly so that there is no wind reversal, the governing equation (3.9) is an elliptic one, and we obtain steady state solutions numerically using the methodology of section 3b. We consider a symmetric mountain profile,

$$h(x) = h_0 e^{-x^2/a^2}, \quad (6.1)$$

with $h_0 = 2$ km and $a = 500$ km. The depth of the incident flow, D, is 10 km with a surface zonal wind, U_0, of 15 m s^{-1}. Taking $N = 10^{-2}$ s^{-1} and $f = 10^{-4}$ s^{-1}, the deformation depth of the mountains, $H_R = fa/N$, is 5 km. With these choices, the mountain Rossby number, $\mathrm{Ro} = U_0/fa$, is 0.3; thus $\mathrm{Ro}^2 = 0.09 \ll 1$ and the semigeostrophic approximation is a relatively good one. The nondimensional mountain and tropopause heights are $\mu = 0.4$ and $z_T = 2$, respectively. In order to ascertain the effect of the shear, we consider three values of $\alpha = \partial U/\partial z$: a forward shear of 15 m s^{-1}/10 km, no shear, and a backward shear of -7.5 m s^{-1}/10 km. Nondimensionally the cases correspond to $\gamma = \frac{1}{2}$, 0, and $-\frac{1}{4}$, respectively. Physically the zonal windspeed at the tropopause is twice its surface value for the forward shear case while it is half that for the backward shear. The next two subsections describe the results for these three cases when the angle of attack is adjusted so that there is no drag. A third subsection examines the consequences of varying this angle.

a. Geostrophic flow fields

The total meridional wind field is displayed in Fig. 3 for these three cases. Antisymmetry of the solution about the origin, $x = 0$, indicates that the drag vanishes in each case. Low-level jets are bound to the slopes of the mountain. Their maximum strengths increase with decreasing shear, being 9.5, 14.0, and 19.1 m s^{-1} for $\gamma = \frac{1}{2}$, 0 and $-\frac{1}{4}$, respectively. In addition, both horizontal and vertical shears increase with decreasing γ. The latter is the relative vorticity, $\zeta = \partial v/\partial x$, and is shown in Fig. 4. Forward shear decreases the strength of the anticyclone at the mountain top while the cyclonic lobes on the slopes are larger and slightly stronger.

Figure 5 displays the dimensional potential temperature for the three cases. In the no shear case, the mountain surface is an isentropic one. In the cases with shear, the lower boundary is nonisentropic. This latter feature is absent in the study of Blumen and Gross (1986). As a consequence, their solutions exhibit no effect of the shear on the geostrophic flow.

Inspection of Fig. 5 indicates two salient features. First, the increase in the static stability of the flow at the mountain top is decreased for forward shear. Second, the shear flow isentropes display a large scale bowing, being convex for the forward shear and concave for the backward shear. This feature reflects the horizontal temperature gradient of the far-field and the permanent turning.

A simple explanation of the reduction of the strength of the geostrophic flow response by positive shear is as follows. Figures 4 and 5 indicate that the response consists of a cold-core mountain anticyclone. In the case without shear, the cold core arises solely from the adiabatic cooling of the fluid parcels as they ascend the mountain ridge. For the forward shear case, the inci-

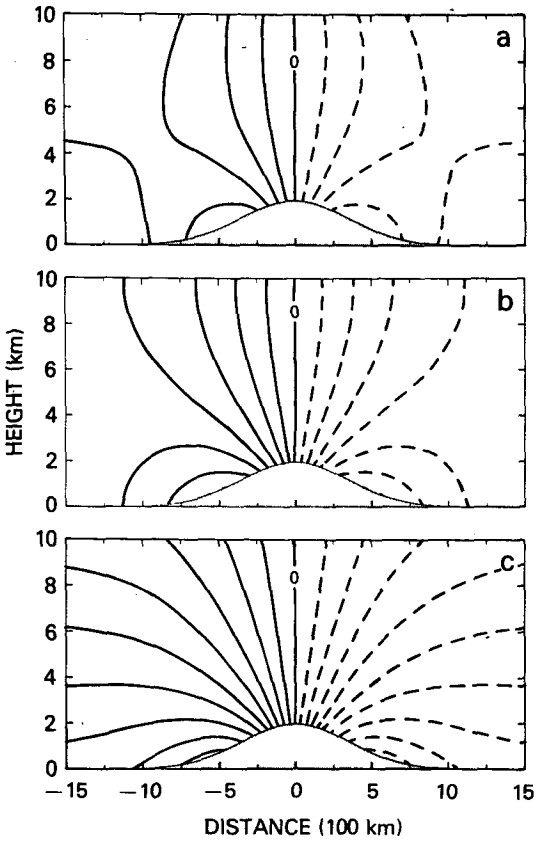

FIG. 3. Contour plots of the total mountain parallel wind, v. The contour interval is 2 m s^{-1}. Negative contours are dashed in this and all subsequent figures. In this figure and Figs. 4–8, panels a, b and c refer to the cases of forward shear ($\gamma = \frac{1}{2}$), no shear ($\gamma = 0$), and backward shear ($\gamma = -\frac{1}{4}$), respectively. The maximum values are 9.5, 14.0, and 19.1 m s^{-1}, respectively.

dent flow has relatively cold air to the north (i.e., positive y-direction) and warmer air to the south. Near the mountain the northward flow on the upslope side produces warm air advection that partially compensates the adiabatic cooling by forced ascent. This weaker cold core implies a reduction in the strength of the anticyclone by the thermal wind relation. In contrast cold air advection in the backward shear case will augment the cooling and produce a stronger anticyclone.

We note that this behavior is not a direct consequence of a change in the potential vorticity, q, of the flow. Defining q dimensionally by

$$q = \frac{g}{\theta_0}(f\hat{z} + \nabla \times \mathbf{v}) \cdot \nabla\theta, \tag{6.2}$$

we find, in the limit as Ro^2 tends to zero,

$$q = fN^2\left[\left(1 + \mu\frac{\partial v}{\partial x}\right)\left(1 + \mu\frac{\partial\theta}{\partial z}\right) - \left(\gamma\epsilon + \mu\frac{\partial v}{\partial z}\right)^2\right]\phi, \tag{6.3}$$

where nondimensional variables are used within the brackets. Far upstream the potential vorticity

$$q = fN^2[1 - \gamma^2\epsilon^2], \tag{6.4}$$

is reduced for both the forward and backward shears.

A convenient measure of the baroclinicity of a flow is the Richardson number, Ri. Dimensionally we define

$$\mathrm{Ri} = \frac{g}{\theta_0}\frac{\partial\theta}{\partial z}\Big/\left[\left(\frac{\partial u}{\partial z}\right)^2 + \left(\frac{\partial v}{\partial z}\right)^2\right]. \tag{6.5}$$

Introducing nondimensional quantities and taking the limit as Ro^2 tends to zero yields

$$\mathrm{Ri} = (1 + \mu\partial\theta/\partial z)\Big/\left(\gamma\epsilon + \mu\frac{\partial v}{\partial z}\right)^2, \tag{6.6}$$

and the zonal wind shear makes no contribution to Ri. Contour plots (Fig. 6) of the Richardson number indicate a reduction of Ri near the mountain, indicating that the increased vertical wind shear dominates the increase in static stability by the mountain. Further, it is seen that the reduction is greater for the case of backward shear. We note that a reduction of Ri tends to stabilize the flow to baroclinic disturbances (Stone 1966) while symmetric instability occurs for Ri < 1.

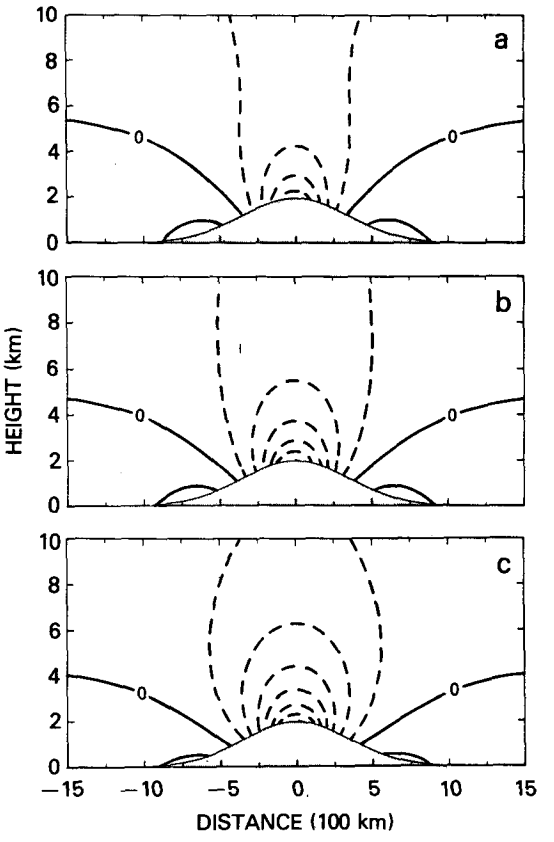

FIG. 4. Contour plots of the vertical component of vorticity, $\zeta = \partial v/\partial x$. The contour interval is 0.8×10^{-5} s^{-1}. The minimum values are (a) $-0.4f$, (b) $-0.5f$, and (c) $-0.6f$.

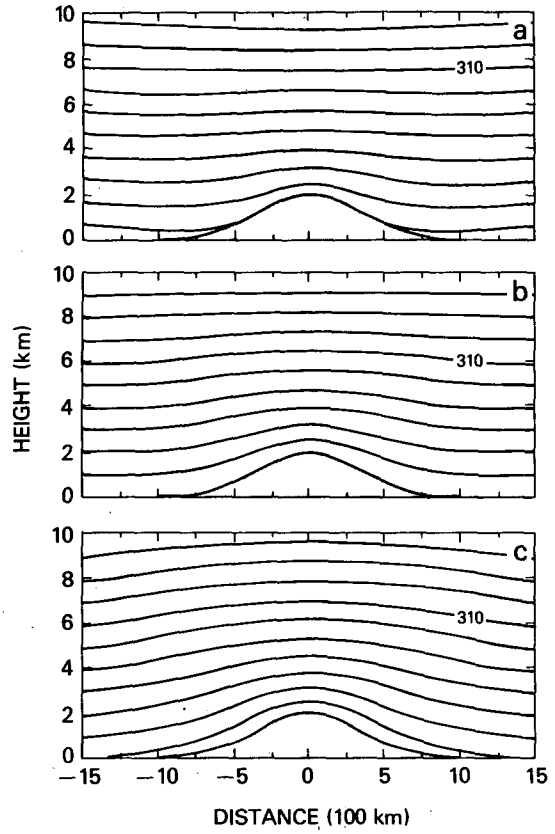

FIG. 5. Contour plots of the potential temperature, θ, in degrees Kelvin. The contour interval is 3 K.

Merkine's (1975) analysis resulted in a net amplification of the shear and hence a net reduction of Ri far downstream of the mountain. The local reduction of Ri displayed in Fig. 6 is a consequence of the oblique angle of attack. A normally incident flow would exhibit a downstream reduction of Ri by the factor A^{-2} where A is given by (4.14).

b. *Ageostrophic flow*

Contour plots of the ageostrophic streamfunction, Φ, [see (4.5) and (4.9)] are shown in Fig. 7. They depict rising motion upstream of the mountain, an ageostrophic wind over the mountain, and sinking motion downstream. The strength of this ageostrophic circulation (as measured by $\Phi_{\min}$ at the mountain top) is -2.7, -3.0, and -3.3 ($\times 10^4$ m^2 s^{-1}) for the backward, no shear, and forward shear cases, respectively. Thus the total ageostrophic mass flux over the peak is larger for forward shear. This is consistent with the fact that there is a greater mass flux incident on the mountain in that case.

Inspection of Fig. 7 indicates that the ageostrophic circulation is much shallower for the backward shear case. As a consequence the maximum ageostrophic wind (Fig. 8) is greater for the backward shear case even though its total mass flux is less. The forward shear case achieves its greater flux at a reduced speed but spread over a greater depth.

The effect of the shear on the ageostrophic flow can be diagnosed by a transverse circulation (or Sawyer-Eliassen) equation. Using standard techniques we find, in the present notation,

$$\left(1+\mu\frac{\partial\theta}{\partial z}\right)\frac{\partial^2\Phi}{\partial x^2}-2\left(\gamma\epsilon+\mu\frac{\partial v}{\partial z}\right)\frac{\partial^2\Phi}{\partial x\partial z}+\left(1+\mu\frac{\partial v}{\partial x}\right)\frac{\partial^2\Phi}{\partial z^2}=-2\gamma\frac{\partial v}{\partial x}. \quad (6.7)$$

The streamfunction Φ must satisfy (6.7) subject to the following boundary conditions:

$$\frac{\partial\Phi}{\partial x}=-\left(\hat{u}+\mu\frac{\partial\Phi}{\partial z}\right)\frac{\partial h}{\partial x} \quad \text{at} \quad z=\mu h(x), \quad (6.8)$$

$$\frac{\partial\Phi}{\partial x}=0 \quad \text{at} \quad z=z_T. \quad (6.9)$$

As is well known, the ellipticity condition for (6.7) is that the potential vorticity (6.3) be positive.

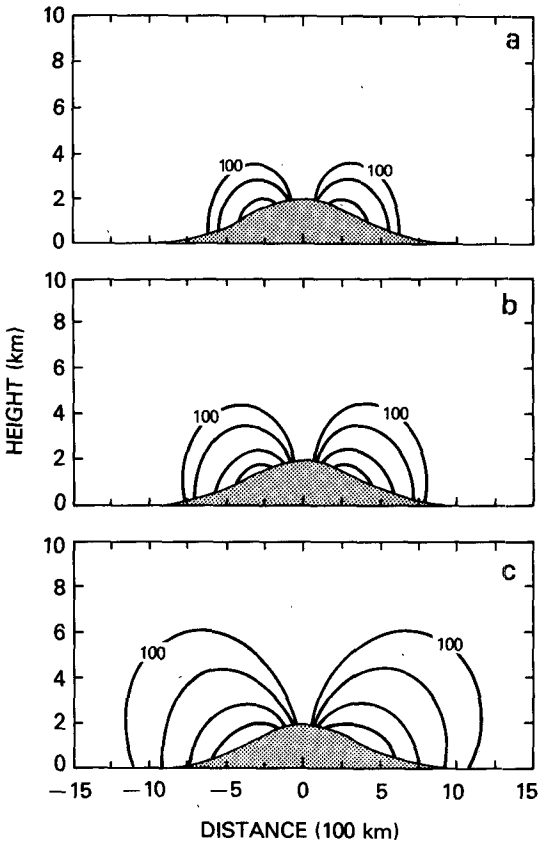

FIG. 6. Contour plots of the Richardson number, Ri, defined by (6.6). The nonuniform contour values are 100, 50, 20, and 10. The minimum value, occurring on the mountain slope, is (a) 14, (b) 8, and (c) 5.

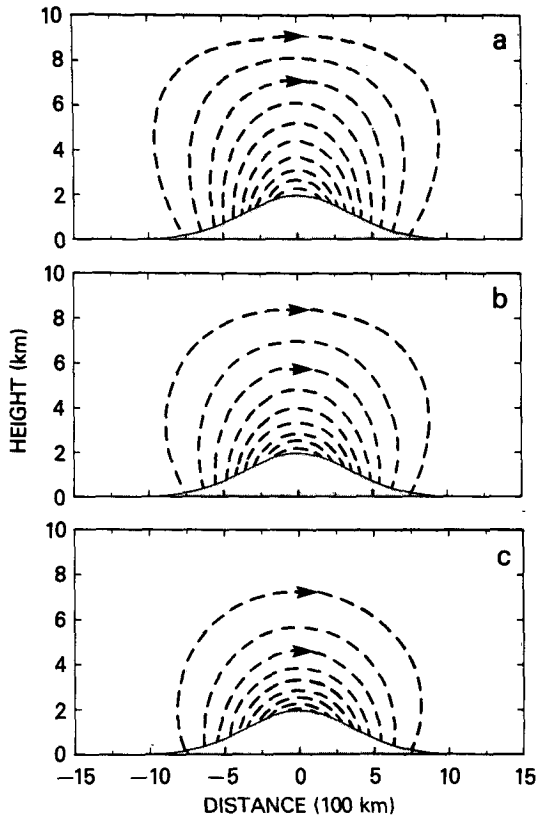

FIG. 7. Contour plots of the ageostrophic stream function, Φ. The contour interval is 3×10^3 m^2 s^{-1}. The minimum value, occurring on the mountain top, is (a) 3.3, (b) 3.0, and (c) 2.7 ($\times 10^4$ m^2 s^{-1}).

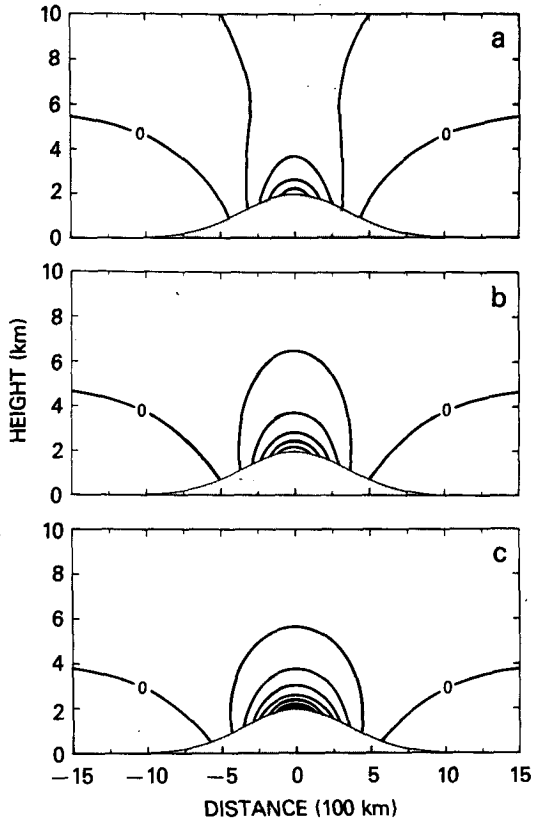

FIG. 8. Contour plots of the ageostrophic zonal wind, u_a. The contour interval is 2.4 m s^{-1}. The maximum value, occurring on the mountaintop, is (a) 11, (b) 14, and (c) 19 m s^{-1}.

The Φ-field is forced by two mechanisms. The first is the mechanical influence of the mountain to induce vertical motions through the lower kinematic boundary condition (6.8). This forcing generates an open-cell circulation that is clockwise in the x–z plane (Fig. 9a) and is greater if $\hat{u}$ increases with height.

The second mechanism is an interior forcing that is represented mathematically by the term on the right-hand side of (6.7). This Q-vector contribution is the sum of differential thermal and momentum advection of equal strength which act to alter the thermal wind balance of the mountain-parallel flow. For forward shear ($\gamma > 0$), this term is positive over the mountain where $\partial v/\partial x$ is negative. A clockwise closed cell circulation (Fig. 9b) is implied for which there is no net transport across the mountain top.

The total Φ-field is the sum of these two contributions since (6.7)–(6.9) is a linear set for Φ. Strictly speaking this set is nonlinear since both forcing mechanisms alter the geostrophic flow and hence the coefficients in (6.7). Such changes, however, are secondary to those discussed here. In the case of forward shear, the closed cell circulation due to the interior forcing will augment the ageostrophic flow aloft but weaken it at mountain top. Thus, the flow is deeper but with a reduced maximum. In contrast, the closed cell circulation for the backward shear case is counterclockwise and the circulation is shallower with an increased maximum. As a consequence, weaker convergence/divergence will occur on the mountain slopes for flow with forward shear. This implies that the frontogenetic character of the mountain-induced flow is reduced for $\gamma > 0$.

The present results indicate that, because the cross-mountain wind is strengthened for backward shear, there will be an earlier breakdown of semigeostrophic theory in this case. Indeed, estimates of the zonal acceleration for Fig. 8c are comparable in magnitude with the corresponding Coriolis acceleration of Fig. 3c. Numerical calculations indicated that the neglected terms

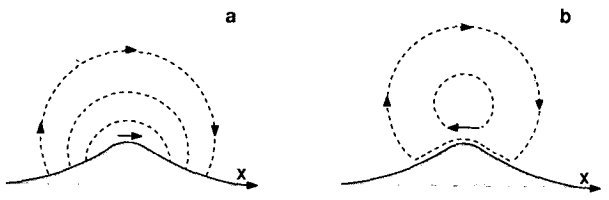

FIG. 9. Schematic presentation of the ageostrophic stream function due to (a) boundary forcing and (b) interior forcing.

(2.9) exceeded in magnitude the retained geostrophic term (2.7a) close to the mountain surface within a small region ($|x| \leq a/2$) of the peak. Thus the criterion (2.10) based on a scale analysis can overestimate the range of validity of the semigeostrophic approximation. Integration of the absolute value of these terms over the lower eighth ($0 \leq z_\infty \leq 0.25$) of the flow near the mountain ($|x| \leq 2a$) showed that the retained term exceeded the neglected ones by a factor of 3.3. Integration of this estimate of the bulk effect of the neglected terms over a deeper layer indicates that the Coriolis term is even more dominant. Furthermore, we note that additional calculations for shallower mountains yielded similar qualitative conclusions regarding the effect of shear on both the geostrophic and ageostrophic flow.

c. *Effect of angle of attack*

The major impact of varying the angle of attack (not shown) is to tilt the axis of both the geostrophic and ageostrophic fields, with incident flow from the southwest (northwest) producing an upstream (downstream) tilt. The tilting of the ageostrophic and vorticity fields in this manner are implied by (6.7) and (4.4), respectively. For a forward shear of $\gamma = 1$, the axes of the fields are displaced a distance of about 250 km at the rigid lid. It is important to note that the tilted vorticity field does not represent a growing/decaying disturbance.

7. Solutions for strong backward shear

This section examines the time development of the flow over a ridge when the background zonal wind has a critical level. The model of ZB is initialized with a zonal flow of surface speed $U_0 = 16$ m s^{-1} and shear $\alpha = -4.0$ m s^{-1}/km. The flow is normally incident (i.e., $\tau = 0$) on the Gaussian ridge (6.1) with width $a = 400$ km. These parameter choices imply $H_R = 4$ km, $\mathrm{Ro}^2 = (0.4)^2 = 0.16$, $\gamma = -1$ and $z_T = 2$.

Initially we let the mountain surface and the tropopause be zonally isentropic surfaces in order to eliminate the starting vortex. Numerical integrations are performed for topography with maximum heights $h_0 = 200$ m and 1 km. For the low mountain, $\mu = 0.05$, the ageostrophic effects are small, and the solution approximates the quasi-geostrophic case. In order to ascertain better the effects of ageostrophy, the low mountain results displayed here are multiplied by a factor of 5 (=1 km/200 m).

Figure 10 shows the pressure perturbation along the surface of the mountain at 6 h intervals during the 24 h integration. Figure 10a shows the normalized pressure perturbation for the low mountain case while Fig. 10b corresponds to the high mountain case. Initially, there is a positive pressure anomaly associated with the mountain anticyclone. Warm advection produces a drop in pressure in the vicinity of the mountain top and the formation of a pronounced pressure trough in the lee of the mountain. This behavior is consistent with the standing baroclinic wave described in Smith's (1984) quasi-geostrophic study. Semigeostrophic effects act to suppress the pressure drop and shift the trough axis downstream.

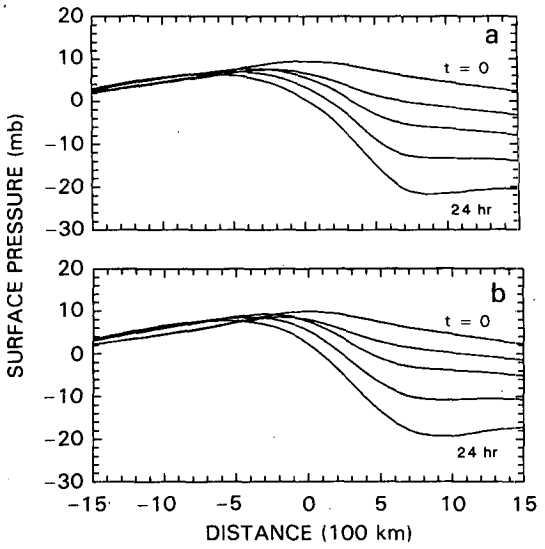

FIG. 10. Time evolution of the surface pressure field as a function of distance across the mountain at six hour intervals for a case of strong backward shear ($\gamma = -1$) with a mountain height of (a) 200 m and (b) 1 km. Results for the low mountain are multiplied by a factor of five.

Figure 11 displays the evolution of the relative vorticity, $\zeta = \partial v_g/\partial x$, along the surface of the mountain. Figure 11a shows the normalized relative vorticity for the low mountain case and Fig. 11b corresponds to the high mountain case. Salient features of the development are an increase in the strength of the mountain anticyclone, consistent with the weak backshear case described in section 6, and the development of an orographically bound region of cyclonic vorticity associated with the leeside orographic trough. Differences between the quasi-geostrophic and semigeostrophic cases are more apparent in these plots. There is little change in the strengthening of the mountain anticyclone between the two cases, with the anticyclone being broader and slightly stronger for the low mountain. Modification of the lee cyclone is more pronounced. The lee cyclone is stronger and narrower for the high mountain. The maximum relative vorticity at 24 h is $\zeta \sim 1.3f$ for the high mountain, compared with a normalized value of $\zeta \sim 0.7f$ for the low mountain. There is also a downstream shift of the vorticity maximum, associated with the shift of the lee pressure trough.

An additional numerical integration for a higher mountain with $h_0 = 2$ km ($\mu = 0.5$) displays a qualitatively similar evolution for the first 12 h of simulated

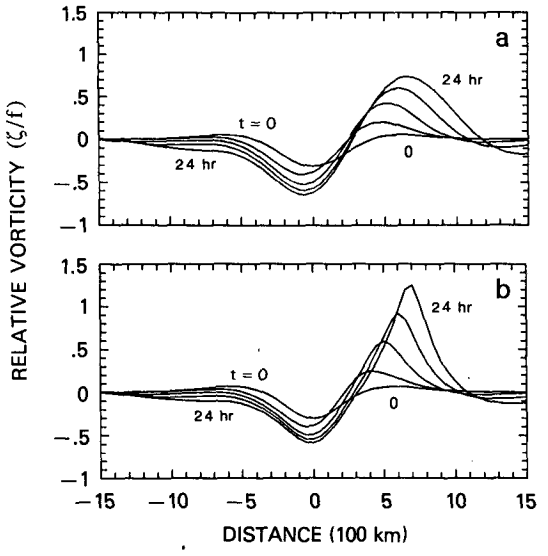

FIG. 11. Time evolution of the surface relative vorticity corresponding to the cases in Fig. 10.

time. At time $t = 12$ h, the relativity vorticity of the lee cyclone is $\zeta = -1.9f$ while that over the mountain is $\zeta = -0.99f$. Subsequently the maximum anticyclonic vorticity $\zeta = -f$ and the transverse circulation equation is no longer elliptic. This point corresponds to the complete breakdown of semigeostrophic theory for which the cross-mountain wind speed is infinite (Pierrehumbert 1985). To demonstrate this correspondence, we write the dimensional version of the meridional momentum equation (2.7b) at the mountain top, where $w = 0$, as

$$(U_M + u_a)\frac{\partial v}{\partial x} + fu_a = 0, \tag{7.1}$$

where $U_M = U_0 + \alpha h_0$. Solving for the ageostrophic zonal wind we obtain

$$u_a = -\frac{U_M \zeta}{(f + \zeta)}. \tag{7.2}$$

Thus, infinite windspeeds at the mountain peak arise concomitantly with the vanishing of the absolute vorticity.

8. Conclusion

We have investigated the flow of a baroclinic current over a mountain ridge in a stratified, uniformly rotating fluid. The problem with the fully nonlinear, nonisentropic lower boundary condition has been solved subject to the semigeostrophic approximation of a geostrophic mountain-parallel flow. Analysis techniques have examined the problem in both a steady, elliptic and an initial-value, hyperbolic context.

Results for the case of forward shear (wind increasing with height) indicate that warm air advection (associated with the ambient thermal gradient) on the upslope side of the mountain partially compensates the adiabatic cooling of the forced ascent. This behavior produces a weaker geostrophic flow field response. In particular, we note that the lack of observational evidence for a large cold anticyclone over synoptic and mesoscale mountain ridges may be explained by this conclusion (see Fig. 12). The effect of forward shear on the ageostrophic flow is to increase the net ageostrophic cross-mountain mass flux but deepen the extent of the circulation so that the maximum ageostrophic winds are reduced. This strengthening of the ageostrophic winds aloft is consistent with the increased permanent turning of the flow aloft. The weakening of the surface ageostrophic wind suggests that the influence of the mountain on the strength and propagation of a front should be decreased proportionately.

Our findings for an incident flow with backward shear (wind decreasing with height) are generally opposite to those for forward shear: the mountain anticyclone is stronger while the ageostrophic circulation is shallower with stronger windspeeds. This strengthening of the ageostrophic winds over the mountain top implies an earlier breakdown of the validity of the semigeostrophic theory used here for cases with backward shear.

A particular contribution of the backward shear cases is the extension of Smith's (1984, 1986) quasi-geostrophic theory of lee cyclogenesis to finite-amplitude topography. It has been shown that the presence of a standing lee wave requires the incident wind to have a critical level. Our numerical solutions to the initial-value problem indicate that ageostrophic processes act to strengthen and narrow the developing lee vortex. However application of the results to the case of cyclogenesis in the lee of the Alps is questionable on two counts. First, the high ($h_0 = 3$ km) and narrow ($a = 300$ km) Alpine topography imply nondimensional parameters [$\mathrm{Ro}^2 = (0.5)^2 = 0.25$ and $\mu = 1.0$], which suggests the breakdown of semigeostrophic theory, thus a nongeostrophic theory is ultimately required. Second, the presence of a persistent critical level is not realistic in many Alpine cyclones.

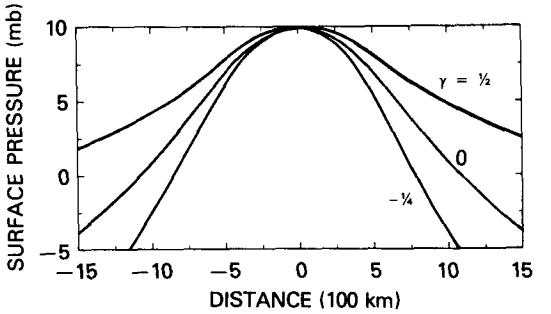

FIG. 12. Surface pressure as a function of distance for three values of the nondimensional shear γ corresponding to the cases of Figs. 3–8.

Acknowledgments. Dr. Pe-Cheng Chu assisted in the analysis described in sections 3a,b. Financial support for PRB in part was provided jointly by the National Science Foundation (NSF) and the National Oceanic and Atmospheric Administration (NOAA) under NSF Grants ATM8606116 and ATM8796245. The elliptic calculations were performed on the computers of the National Center for Atmospheric Research (NCAR) which is sponsored by NSF. JAZ was supported by a National Research Council-National Aeronautics and Space Administration Research Associateship.

APPENDIX

The Quasi-geostrophic Case

In the quasi-geostrophic situation, the dynamics are governed by the conservation of potential vorticity of the form:

$$\hat{u}\frac{\partial}{\partial x}\left[\frac{\partial^2\phi}{\partial x^2}+\frac{\partial^2\phi}{\partial z^2}\right]=0, \tag{A1}$$

$$w=\begin{cases}\hat{u}\partial h/\partial x & \text{at} \quad z=0, \qquad \text{(A2)}\\ 0 & \text{at} \quad z=z_T. \qquad \text{(A3)}\end{cases}$$

The vertical motion field is related to the geopotential by the heat equation:

$$w=\gamma\frac{\partial\phi}{\partial x}-\hat{u}\frac{\partial}{\partial x}(\partial\phi/\partial z). \tag{A4}$$

The solution may be found using Fourier transform techniques to be

$$v(x,z)=\frac{\partial\phi}{\partial x}$$

$$=\mathrm{Re}\int_{-\infty}^{+\infty} ik\,\frac{H(k)e^{ikx}\mathcal{N}(k,z)}{\mathcal{D}(k,z_T)}\,dk, \tag{A5}$$

where $H(k)$ is the Fourier transform of the mountain profile $h(x)$ and

$$\mathcal{N}(k,z)=k\cosh k(z-z_T)+\gamma'\sinh k(z-z_T), \tag{A6}$$

$$\mathcal{D}(k,z_T)=(k^2-\gamma\gamma')\sinh kz_T + k(\gamma-\gamma')\cosh kz_T, \tag{A7}$$

$$\gamma'=\gamma/(1+\gamma z_T)=\gamma/\hat{u}_T. \tag{A8}$$

The far-field ($|x|\to\infty$) behavior of v is dominated by the contribution of the poles of the integrand. In particular, a pole at $k=0$ will contribute the permanent turning while a nonzero pole represents a sinusoidal stationary lee wave disturbance. By the principles of contour integration, we find that

$$\Delta\bar{v}=v(x=+\infty,z)-v(x=-\infty,z)$$

$$=2\pi i(\text{Residue at } k=0), \tag{A9}$$

where the overbar denotes a "mean" turning in which the lee wave contributions are neglected. Taylor series expansion about $k=0$ of the hyperbolic functions in (A6) and (A7) enables the residue of the integrand to be determined. The result is

$$\Delta\bar{v}=-\frac{2\pi H(0)\hat{u}}{z_T[1+\gamma z_T+(\gamma^2 z_T^2/3)]}. \tag{A10}$$

Since $2\pi H(0)$ is the mountain volume, (A10) is identical to (4.10) with $\mu=0$.

We next examine under what conditions lee waves may exist. Poles of the integrand in (A5) occur when there are zeros in the denominator. Setting $\mathcal{D}(k,z_T)=0$ yields

$$\tanh K=\frac{-K_c^2 K}{K^2-K_c^2}, \tag{A11}$$

where $K=kz_T$ and $K_c^2=\gamma^2 z_T^2/U_T$. Regardless of the direction of the shear, (A11) has the root $k=0$ which provides the permanent turning. For positive shear or weak backshear for which $U_T=1+\gamma z_T>0$, $K_c^2>0$, and only the $k=0$ root exists. For strong backshear, $K_c^2<0$, and stationary lee waves exist provided

$$\frac{\gamma^2 z_T^2}{(-U_T)}\geqslant 3.01.$$

This criterion is always met for a semi-infinite model atmosphere (Smith 1984).

REFERENCES

Bannon, P. R., 1985: Flow acceleration and mountain drag. *J. Atmos. Sci.*, **42**, 2445–2453.

——, and P. C. Chu, 1988: Anelastic semigeostrophic flow over a mountain ridge. *J. Atmos. Sci.*, **45**, 1020–1029.

Blumen, W., 1988: Stratified, rotating flow over orography: The rigid-lid boundary condition and the far-field circulation. *J. Atmos. Sci.*, **45**, 1417–1422.

——, and B. D. Gross, 1986: Semigeostrophic disturbances in a stratified shear flow over a finite-amplitude ridge. *J. Atmos. Sci.*, **43**, 3077–3088.

Hayes, J. L., R. T. Williams and M. A. Rennick, 1987: Lee cyclogenesis. Part I: Analytic studies. *J. Atmos. Sci.*, **44**, 432–442.

Jacobs, S. J., 1964: On stratified flow over bottom topography. *J. Mar. Res.*, **22**, 223–235.

Mattocks, C., and R. Bleck, 1986: Jet streak dynamics and geostrophic adjustment during the initial stages of lee cyclogenesis. *Mon. Wea. Rev.*, **114**, 2033–2056.

Merkine, L. O., 1975: Steady finite-amplitude baroclinic flow over long topography in a rotating stratified atmosphere. *J. Atmos. Sci.*, **32**, 1881–1893.

Pierrehumbert, R. T., 1985: Stratified semigeostrophic flow over two-dimensional topography in an unbounded atmosphere. *J. Atmos. Sci.*, **42**, 523–526.

Robinson, A. R., 1960: On two-dimensional inertial flow in rotating stratified fluid. *J. Fluid Mech.*, **9**, 321–332.

Smith, R. B., 1979: Some aspects of the quasi-geostrophic flow over mountains. *J. Atmos. Sci.*, **36**, 2385–2393.

——, 1984: A theory of lee cyclogenesis. *J. Atmos. Sci.*, **41**, 1159–1168.

——, 1986: Further development of a theory of lee cyclogenesis. *J. Atmos. Sci.*, **43**, 1582–1602.

Stone, P. H., 1966: On non-geostrophic baroclinic stability. *J. Atmos. Sci.*, **23**, 390–400.

Zehnder, J. A., and P. R. Bannon, 1988: Frontogenesis over a mountain ridge. *J. Atmos. Sci.*, **45**, 628–644.